文章编号：1001-9014(2023)02-0260-07

DOI:10.11972/j.issn.1001-9014.2023.02.017

Modeling and analysis for imaging characteristics of infrared array-aperture diffractive optical system

NIU Rui-Ze[1], QIAO Kai[2], ZHI Xi-Yang[1*], GONG Jin-Nan[1], JIANG Shi-Kai[1], TIAN Chao[3]

(1. Research Center for Space Optical Engineering, Harbin Institute of Technology, Harbin 150001, China;
2. Beijing Institute of Tracking and Telecommunications Technology, Beijing 100094, China;
3. School of Computer Science and Technology, Harbin Institute of Technology, Shenzhen 518000, China)

Abstract: This paper establishes the modulation transfer function (MTF) and signal-to-noise ratio (SNR) characterization models of the infrared array-aperture diffractive optical system based on the diffraction imaging mechanism. Subsequently, the imaging system diffraction efficiency is calculated based on the three-dimensional Finite Difference Time Domain (FDTD) method and the imaging characteristics are represented by combining the MTF and SNR. Finally, the effects of different working wavelengths, field of views and filling factors of the primary lens imaging characteristics are analyzed. The analysis results show that the diffraction efficiency, the MTF and SNR of infrared array-aperture diffractive optical system all have spectral and spatial variation characteristics, which reduce with the decrease of the primary lens filling factor. When the filling factor is 0.6, the integral area of MTF decreases by 45.42% and the *SNR* decreases by 4.92 dB compared with the ideal full aperture system. The established model can be used to characterize the imaging quality of infrared array-aperture diffractive optical system and provide reference to the imaging system design.

Key words: optical remote sensing, infrared array-aperture diffractive optical system, diffraction efficiency, finite difference time domain

红外合成孔径衍射光学系统成像特性建模与分析

牛锐泽[1], 乔 凯[2], 智喜洋[1*], 巩晋南[1], 江世凯[1], 田 超[3]

(1. 哈尔滨工业大学 空间光学工程研究中心,黑龙江 哈尔滨 150001;
2. 北京跟踪与通信技术研究所,北京 100094;
3. 哈尔滨工业大学(深圳) 计算机科学与技术学院,广东 深圳 518000)

摘要:基于衍射成像机理,建立红外合成孔径衍射光学系统调制传递函数(MTF)和信噪比(SNR)模型。随后,基于三维时域有限差分(FDTD)方法计算成像系统衍射效率,进而结合调制传递函数与信噪比表征系统成像特性。最后,分析了不同工作波长、视场和填充因子对主镜成像特性的影响。分析结果表明,红外合成孔径衍射光学系统的衍射效率、MTF和信噪比均具有空变、谱变特性,且随主镜填充因子的减小而降低。当填充因子为0.6时,与理想的全孔径系统相比,MTF积分面积降低45.42%,信噪比减小4.92 dB。该模型可用于分析红外合成孔径衍射光学系统成像质量,为成像系统的设计提供参考。

关 键 词:光学遥感;红外合成孔径衍射光学系统;衍射效率;时域有限差分

中图分类号:O439　　**文献标识码**:A

Introduction

The high-resolution GEO satellites realize continuous observation of specific areas, which are of great significance in disaster relief, resource exploration and military reconnaissance. GEO satellites put forward new re-

Received date: 2022-10-24, **revised date**: 2022-12-21　　**收稿日期**:2022-10-24,**修回日期**:2022-12-21

Foundation items: Supported by the National Natural Science Foundation of China under Grant 61975043 and 61605035.

Biography: NIU Rui-Ze (1996-), female, Harbin China, Ph. D. Reseach area involves remote sensing image information processing. E-mail: 15636822709@163.com

* **Corresponding author**: E-mail: zhixiyang@hit.edu.cn

quirements for space optical imaging technology, such as lightweight and foldable. Some new optical imaging technologies arise accordingly[1-3]. In particular, the array-aperture diffractive optical system uses membrane as the primary lens, which can be folded easily and has the advantage of ultra-light weight, becoming one of the most potential development directions of space diffractive optical system.

Some researches have been conducted on the array-aperture diffractive optical system. Lawrence Livermore National Laboratory (LLNL) launched the Eyeglass project in 1999[4]. This project designed the folding/unfolding structure, and manufactured 5 m aperture array-aperture diffractive optical system to carry out ground experiments[5]. The Membrane Optical Imager Real-time Exploitation (MOIRE) was completed by the Defense Advanced Research Projects Agency (DARPA) in 2010[6-7]. Its array-aperture primary lens is up to 20 m, which can ensure the resolution higher than 2.5 m and the imaging time less than 1s. The instantaneous field of view (FOV) covers more than 10 km ×10 km and the total detection area is greater than 10 000 km ×10 000 km[8-10].

However, compared with the traditional refractive/reflective full-aperture system, the array-aperture primary lens decreases the modulation transfer function (MTF) and the focal plane energy[11]. Meanwhile, the diffraction imaging reduces the resolution and contrast[12-15]. Impacted by the coupling effect of primary lens structure and diffraction imaging, the infrared array-aperture diffractive optical system presents new imaging characteristics, which have rarely been reported. Consequently, it is necessary to analyze the imaging degradation characteristics of the infrared array-aperture diffractive optical system.

In this paper, we build the MTF and signal-to-noise ratio (SNR) models to express the spatial frequency modulation and energy transmission characteristics separately by considering the comprehensive influence of array-aperture structure and diffraction imaging. Furthermore, we present a fast method to solve the diffraction efficiency based on Finite Difference Time Domain (FDTD) according to the subwavelength micro structure of the array-aperture primary lens surface. This work can be applied to analyze the imaging quality and provide reference to the design of the infrared array-aperture diffractive imaging system.

1 Experiments

The imaging mechanism of infrared array-aperture diffractive optical system is shown in Fig. 1. The light passes through the array-aperture diffractive primary lens, which expands the FOV of the optical system with lightweight structure. Then the refraction lenses are used to aggregate the light to achieve high-resolution imaging, between which added the corresponding diffraction lens to eliminate the chromatic aberration.

The primary lens of the system is constituted with array-aperture Fresnel diffractive lenses, which modulate incident light through surface microstructure to achieve imaging. We analyze the light field distribution in the focal plane by calculating the diffraction efficiency, which

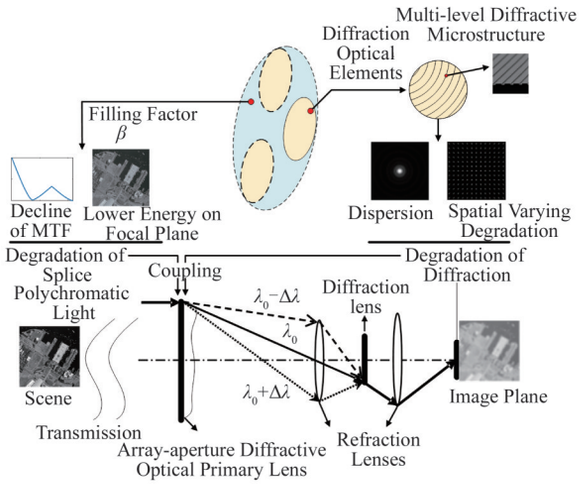

Fig. 1 Mechanism of degradation
图1 成像机理

is the important index to characterize the imaging quality of the diffraction system. The diffraction efficiency is defined as the ratio of the energy within the airy spot zero-order to the total incident energy[12]:

$$\eta = \frac{\int_0^{2\pi}\int_0^{a}\left|E_{focal}(r,\theta)\right|^2 drd\theta}{\int_0^{2\pi}\int_0^{D/2}\left|E_{inc}(r,\theta)\right|^2 drd\theta}, \quad (1)$$

where $E_{focal}(r,\theta)$ and $E_{inc}(r,\theta)$ are the energy distribution in the focal plane and incident plane respectively.

Nevertheless, due to the diffractive element microstructure and the total reflection, a part of incident light cannot converge to the focus limited by the deflection angle, resulting in the decline of diffraction efficiency. This phenomenon is the shadow effect in continuous phase structure, whose mechanism is shown in Fig. 2[16]. In the normal incidence, the degree of continuous phase Fresnel lens upper surface inclination intensifies gradually by the lateral band width decreasing, resulting in the increase of incident angle. When the incident angle increases until the total reflection occurs, the incident energy losses. And in the case of oblique incident, the partial incident light is parallel to the optical axis, which forms stray radiation in the focal plane, reducing the diffraction efficiency of the Fresnel lens[17].

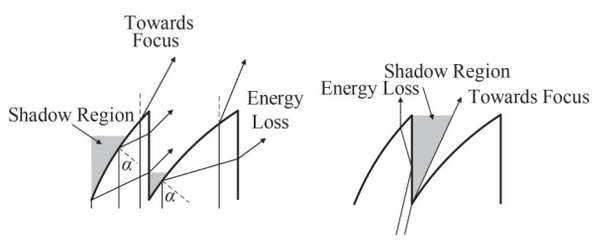

Fig. 2 Shadow effects in continuous phase structure,(a) normal incidence, (b) oblique incidence
图2 连续相位结构中阴影效应,(a)正入射,(b)斜入射

The Shadow effect on the Fresnel lens multi-level micro structure with four steps is shown as Fig. 3. For

the outer ring, when the deflection angle of incident light gradually increases, the tolerance of element microstructure for the emergence angle β decreases gradually, which makes the energy loss in the focal plane and the decline of diffraction efficiency.

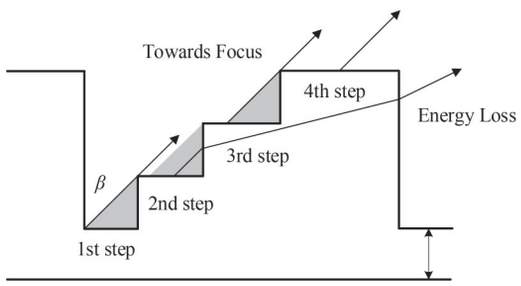

Fig. 3 Shadow effects in multi-level structure
图3 多台阶结构阴影效应

Based on the above analysis, the infrared array-aperture diffractive optical system has lower energy on image plane compared to the full aperture system. Simultaneously, the limit of diffractive microstructure for incident light makes the diffraction efficiency decreases gradually at the outer rings of the primary lens. In addition, the intermediate frequency information reduces due to the sparseness of array-aperture structure. These factors makes the imaging degradation characteristics more complex. From the perspective of spatial frequency modulation and energy transmission, we choose *MTF* and *SNR* to characterize the quality degradation of images, and establish the coupled degradation model of the infrared array-aperture diffractive optical system.

1.1 Analysis model of MTF

The entrance pupil of primary lens contains several identical circular apertures arranged in certain structure instead of whole connected domain. Typical infrared array-aperture structures include Golay3, Ring6 and Triarm7. The generalized pupil function of primary lens can be expressed as:

$$P_{Array}(x,y) = circ\left(\frac{\sqrt{x^2+y^2}}{d/2}\right)\cdot\sum_{i=1}^{N}\delta(x-x_i,y-y_i), \quad (2)$$

where $circ(\cdot)$ is circular function, d is the diameter of the sub-aperture, (x_i, y_i), N are the center coordinate and number of sub-apertures separately.

According to the scalar diffraction theory, the Point Spread Function (*PSF*) and the *MTF* of the primary lens can be obtained with Eq. 3 and Eq. 4.

$$PSF_{Array} = \left|\mathcal{F}\left\{P_{Array}\right\}\right|^2 , \quad (3)$$

$$MTF_{Array} = \left|\mathcal{F}\left\{PSF_{Array}\right\}\right| , \quad (4)$$

where $\mathcal{F}\{\ \}$ represents the Fourier transform function, and $|\ |$ is the modulus operator. By combining Eq. 2, Eq. 3 and Eq. 4, the MTF of the primary lens can be expressed as:

$$\begin{cases} MTF_{Array}(f_x,f_y) = MTF_{Sub}(f_x,f_y) + \frac{1}{N}MTF_{Sub}(f_x,f_y)\cdot \sum_{n=1}^{N(N-1)/2}\delta(f_x \pm \frac{\Delta x_n}{\lambda d_i}, f_y \pm \frac{\Delta x_y}{\lambda d_i}) \\ MTF_{Sub}(f_x,f_y) = \begin{cases} \frac{2}{\pi}\left[\cos^{-1}(\frac{\rho}{\rho_{dc}}) - \frac{\rho}{\rho_{dc}}\sqrt{1-(\frac{\rho}{\rho_{dc}})^2}\right], \\ 0 < \rho < \rho_{dc} \\ 0, \rho \geqslant \rho_{dc} \end{cases} \end{cases} , \quad (5)$$

where MTF_{Array} and MTF_{Sub} represent the *MTF* of the primary lens and array apertures respectively, $(\Delta x_n, \Delta y_n)$ is the relative coordinates of n-th pair of array apertures, d_i is the distance from exit pupil to image plane, $f_x = x/\lambda d_i$, $f_y = y/\lambda d_i$ are spatial frequency, $k = 2\pi/\lambda$, $r_1 = \sqrt{x^2+y^2}$ is the radial coordinate, $\rho = \sqrt{f_x^2+f_y^2}$, and $\rho_{dc} = d/\lambda d_i$ is the cut-off frequency of array apertures.

The MTF_{Sub} decreases when the array apertures get sparse. Meanwhile, the relative coordinates of array apertures $(\Delta x_n, \Delta y_n)$ increase, which makes the secondary peak of MTF_{Array} move laterally and the MTF_{Array} decrease. We define the filling factor to represent the sparsity of array apertures, which can be expressed as[18]:

$$\beta = \frac{Nd^2}{D^2} , \quad (6)$$

where D is the equivalent aperture of the infrared array-aperture primary lens, which is defined as the maximum circumscribed circle diameter of each aperture.

Equation 5 illustrates the traditional initial estimates of MTF for the ideal primary lens, which only considers the effect of aperture diffraction limit. However, it doesn't take the diffraction efficiency into account which is called the initial *MTF* consequently. We take the diffraction efficiency into consideration to modify the initial MTF, establishing the MTF model of infrared array-aperture diffractive optical system. Based on the existing research[19], the energy of non-designated in frequency domain can be considered to be an impulse function. The optical transfer function (OTF) and MTF of the infrared array-aperture diffractive optical system can be expressed as Eq. 7 and Eq. 8[13]:

$$\begin{aligned} OTF(f_x,f_y) &= \eta_{int}\frac{\int_{-\infty}^{\infty}\int_{-\infty}^{\infty}P_1(u,v)\otimes P_1(u,v)dudv}{\int_{-\infty}^{\infty}\int_{-\infty}^{\infty}|t_1(u,v)|^2 dudv} + \\ &(1-\eta_{int})\delta(x)\delta(y) \\ &= \eta_{int}\cdot MTF_{Array}(f_x,f_y) + (1-\eta_{int})\delta(x)\delta(y) \end{aligned} , \quad (7)$$

$$MTF(f_x,f_y) = \left|OTF(f_x,f_y)\right| , \quad (8)$$

where $P_1(\ )$ and $t_1(\ )$ is the pupil function and transmittance function of designated light respectively, η_{int} is the integral diffraction efficiency, which can be calculated by Eq. 1.

1.2 Analysis model of SNR

The SNR is an important index in the imaging performance evaluation of the optical system, which can represent the energy utilization efficiency. It can be defined as[20]:

$$SNR = 10\lg\left[\frac{\mathrm{var}(g)}{\sigma^2}\right] \quad , \quad (9)$$

where $\mathrm{var}(g)$ and σ^2 are variance of signal and noise respectively. The σ^2 includes a variety of independently distributed noises, which can be expressed as:

$$\begin{aligned}\sigma^2 &= \left(G^2\sigma^2_{\mathrm{dark}} + G^2\sigma^2_{\mathrm{readout}} + G^2\sigma^2_{\mathrm{PATTERN}}\right) + \sigma^2_{CHIP} + \\ &\quad \sigma^2_{\mathrm{ADC}} + \sigma^2_{\mathrm{shot}} \\ &= \sigma^2_{\mathrm{shot}} + \sigma^2_{Others}\end{aligned} \quad , \quad (10)$$

where G is the gain, σ_{dark}, $\sigma_{readout}$, $\sigma_{\mathrm{PATTERN}}$, σ_{CHIP} and σ_{ADC}represent the noise of dark current, the readout noise, the mode noise, the amplifier noise and the quantization noise separately. Particularly, σ_{shot} is the grainy noise, which is related to the total energy of incident light.

Subsequently, we analyze the energy in the focal plane of the infrared array-aperture diffractive optical system. The illuminance E of the radiation source on the image plane ds' can be expressed as:

$$E = \frac{\Phi'}{ds'} = \frac{K\Phi}{ds'} = \frac{KLds\Omega}{ds'} = KL\beta_c\frac{S}{r^2} \quad , \quad (11)$$

where Φ, Φ' are the luminous flux on the object and image plane separately, K is the transmittance, L is the radiation brightness, ds is the radiation source on object plane, Ω is the solid angle of entrance pupil. $\beta_c = ds/ds'$, which is defined as the lateral magnification of optical system, $\Omega = S/r^2$, S is the area of the entrance pupil and r is the object distance.

As for the infrared array-aperture diffractive optical system, the energy of non-designated order cannot be used in imaging. Equation 11 can be modified as:

$$E = K\eta_{\mathrm{int}}L\beta_c\frac{\sum_i S_i}{r^2} \quad , \quad (12)$$

where η_{int} is the integral diffraction efficiency, Si is the area of i–th sub-aperture, $S = \sum_i S_i$.

The effective energy Q_1 received by detector on the focal plane of the infrared array-aperture diffractive optical system can be expressed as:

$$Q_1 = EAt = AtK\eta_{\mathrm{int}}L\beta_c\frac{\sum_i S_i}{r_1{}^2} \quad , \quad (13)$$

where A is the pixel area, t is the integration time.

And the energy Q_2 received by detector on the focal plane of the equivalent full-aperture optical system can be calculated as:

$$Q_2 = AtKL\beta_c\frac{S_2}{r_2{}^2} \quad . \quad (14)$$

When r_1=r_2:

$$\frac{Q_1}{Q_2} = \frac{\eta_{\mathrm{int}}\sum_i S_i}{S_2} = \eta_{\mathrm{int}}\beta \quad . \quad (15)$$

Assuming the detector output is a linear response to the incident light energy, the SNR of the infrared array-aperture diffractive optical system can be written as:

$$\begin{aligned}SNR &= 10\lg\left[\frac{\mathrm{var}\left(\eta_{\mathrm{int}}\beta g_0\right)}{\sigma^2_{Others} + \beta\sigma^2_{shot}}\right] = 10\lg\left[\frac{\left(\eta_{\mathrm{int}}\beta\right)^2\mathrm{var}\left(g_0\right)}{\sigma^2_{Others} + \beta\sigma^2_{shot}}\right] \\ &= 10\lg\left[\frac{\beta^2\,\mathrm{var}\left(g_0\right)}{\sigma^2_{Others} + \beta\sigma^2_{shot}}\right] + 20\lg\eta_{\mathrm{int}} \\ &= SNR_\beta + 20\lg\eta_{\mathrm{int}}\end{aligned} \quad , \quad (16)$$

where g_0 is the output energy of the full-aperture optical system and SNR_β is the SNR of infrared array-aperture primary lens under the condition of 100% diffraction efficiency.

1.3 Solution of diffraction efficiency

It can be seen from Sects. 1.1 and 1.2 that calculating the diffraction efficiency is the significant process of solving the MTF and SNR model. For the infrared array-aperture diffractive optical system, the size of the primary lens diffraction microstructure is in subwavelength level. The coupling effect of electromagnetic field components on the primary lens discontinuous microstructure surface enhances. In the circumstances, the vector diffraction theory should be applied for analysis instead of the scalar diffraction theory. For the non-rotational symmetry structure of the infrared array-aperture diffractive primary lens, we apply the Finite Difference Time Domain (FDTD) method to solve the diffraction efficiency based on the vector diffraction theory.

As shown in Fig. 4, the primary lens and wave source are located in the computational space and connection boundary separately. We adopt the time-harmonic field source as the plane wave source and the perfectly matched layer (PML) as the absorption boundary of FDTD calculation. Particularly, PML is a special propagation medium, whose wave impedance is equal to that of the adjacent medium in the calculation space with electromagnetic waves decaying rapidly.

Limited by computing resource, the FDTD method can only acquire the light field distribution on the output plane near the primary lens. When the light field in computational space reaches the steady state, we apply the vector-based plane-wave spectrum (VPWS) method to obtain the light field distribution in the focal plane and compute the diffraction efficiency of primary lens[21]. The process of solving diffraction efficiency is shown in Fig. 5.

2 Results and discussions

2.1 Experimental settings

In this section, the proposed model and method are verified and analyzed through experiments. We consider a certain infrared array-aperture diffractive optical system to analyze the influences of wavelength, FOV and filling factor on diffraction efficiency. Further, we take the diffractive optical system design parameters as the input to analyze the variation of MTF and *SNR* at different wavelengths, FOV and filling factor based on the established analysis model. Finally, we verify the validity of model by comparing with the theoretical analysis results

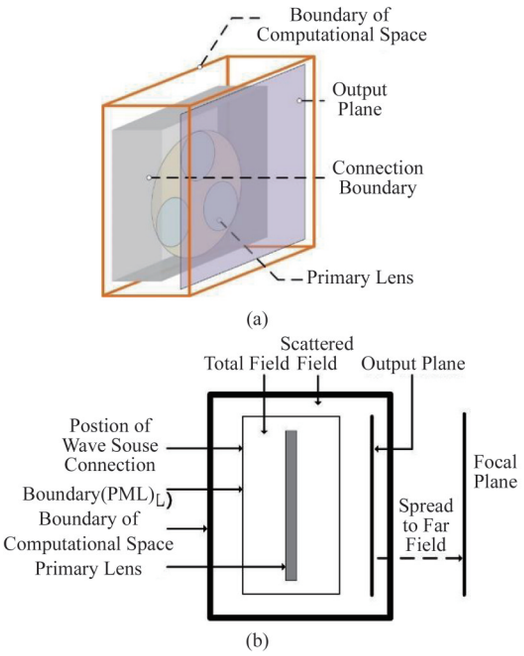

Fig. 4 Schematic of FDTD analysis, (a) 3D schematic, (b) side view of schematic
图4 FDTD原理图, (a) 3D原理图,(b)侧视图

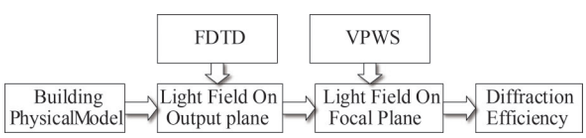

Fig. 5 Flow to solve diffraction efficiency
图5 衍射效率计算流程

in Sect. 1, and provide suggestions for infrared array-aperture diffractive optical system design.

We select the Golay3 structure to design the primary lens in Fig. 6, which is the most classical and representative structure of the infrared array-aperture diffractive optical system. The design parameters of system are shown in Table 1. Declaratively, base thick refers to the thickness at the thinnest position of the primary lens.

In addition, in order to calculate the imaging system diffraction efficiency accurately and efficiently, we adopt the time harmonic plane wave with amplitude of 1 as the incident wave source, and set the space step and the thickness of PML layer as λ/20 and 8 grids respectively.

2.2 Experimental results and analysis

(1)Influence of filling factor on the primary lens imaging characteristics

First, we carry out experiments to explore the influence of filling factor on the imaging characteristics in the infrared array-aperture diffractive optical system. The primary lens array-aperture structure and the central section of Airy spots with different filling factor are shown in

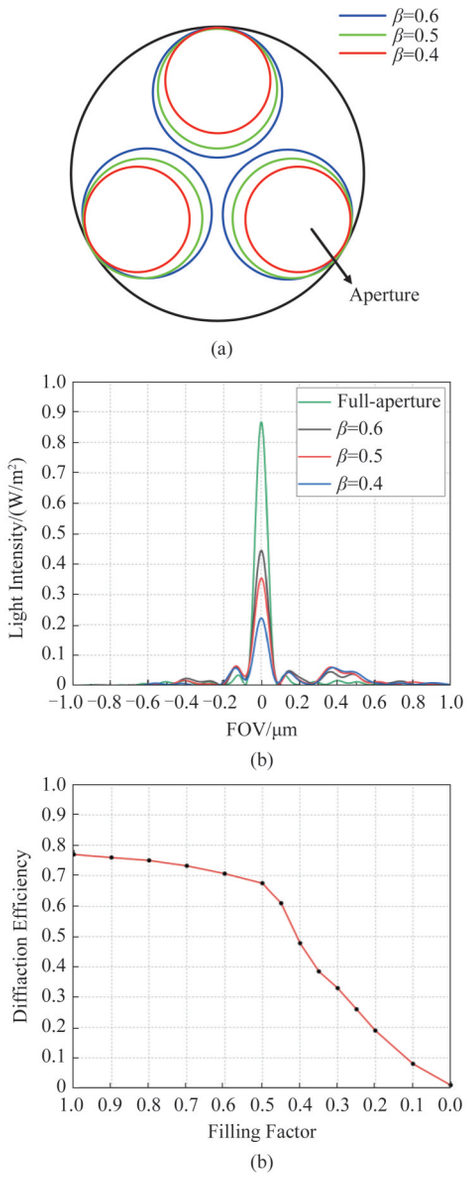

Fig. 6 Infrared array-aperture structure and Airy spot profile with different filling factors, (a) infrared array-aperture structure, (b) focal plane energy distribution of different filling factors, (c) diffraction efficiency curve
图6 不同填充因子红外合成孔径结构及艾里光斑剖面, (a)红外合成孔径结构,(b)不同填充因子焦平面能量分布,(c)衍射效率变化曲线

Fig. 6(a) and (b) successively. When β are 0.6, 0.5 and 0.4, the diffraction efficiencies are 70.68%, 67.51% and 47.81 % respectively. In addition, we plot the diffraction efficiency curve with filling factor variation in Fig. 6(c). Thus the filling factor can be selected according to the actual requirements in engineering applications. It can be seen that the diffraction efficiency decreases rapidly by the decline of the filling factor, which

Table 1 Simulation parameters of the infrared array-aperture diffractive primary lens
表1 红外合成孔径衍射主镜仿真参数

Wavelength	Refractive index n	Focal length f	F number	Number of steps	Stitching structure	Fill factor	Base thick
900~980 nm	1.5	10 mm	1.43	4	Golay3	0.4~0.6	0.45 μm

caused by the decrease of the light convergence ability at the outer rings with high gate density.

According to the MTF analysis model established in Sect. 1.1, Fig. 7 shows the MTF curves in the meridian direction of central FOV with different filling factors. The array-aperture structure causes the side lobe effect, which leads to the mutation point in the MTF curve. Compared with the ideal equivalent full aperture system, the MTF area decreases by 45.42%, 54.49% and 66.10% respectively. Accordingly, the decrease in filling factor leads to the weakening of image plane energy and the reduction of diffraction efficiency.

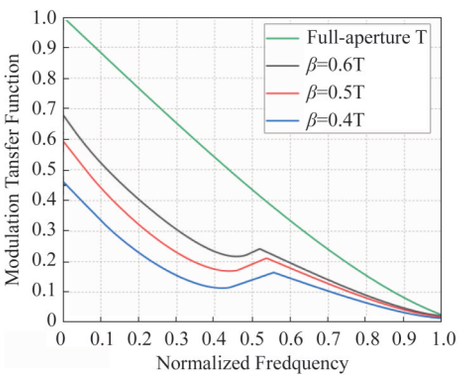

Fig. 7 MTF in the central FOV with different filling factors
图7 不同填充因子中心视场MTF

Meanwhile, according to the SNR characteristic analysis model established in Section 1.2, when β are 0.6, 0.5 and 0.4 respectively, the SNR of the system decreases by 4.92 dB, 6.85 dB and 9.63 dB compared with the ideal full aperture system by considering the particle noise simply. Ulteriorly, due to the existence of other noises such as dark current noise, the SNR will decrease more violently with the filling factor decreasing.

(2) Influence of wavelength and FOV on the primary lens imaging characteristics

In order to further verify the correctness of the proposed model, we analyze the effects of different wavelength and FOV on the imaging characteristics. Figure 8 (a) shows the irregular central profiles of the Airy spot with the incident light wavelengths of 900 nm, 950 nm and 980 nm. The diffraction efficiencies are 70.68%, 64.16% and 50.95% respectively. Figure 8 (b) shows the irregular central profiles of the Airy spot when the incident wavelength is 900 nm and the FOVs are 0°, 3° and 5° respectively. Correspondingly, the diffraction efficiencies are 70.68%, 69.35% and 65.71%.

Meanwhile, we analyze the degradation characteristic of MTF at different incident wavelengths and FOVs in Fig. 9. Table 2 shows the decreasing degree of the *SNR* and MTF area of the central FOV at different wavelengths and FOVs compared with the ideal full aperture system.

Summarily, for the infrared array-aperture diffractive system, the center FOV has the optimal imaging quality. While with the deviations of wavelength and FOV, the diffraction efficiency, the MTF and SNR de-

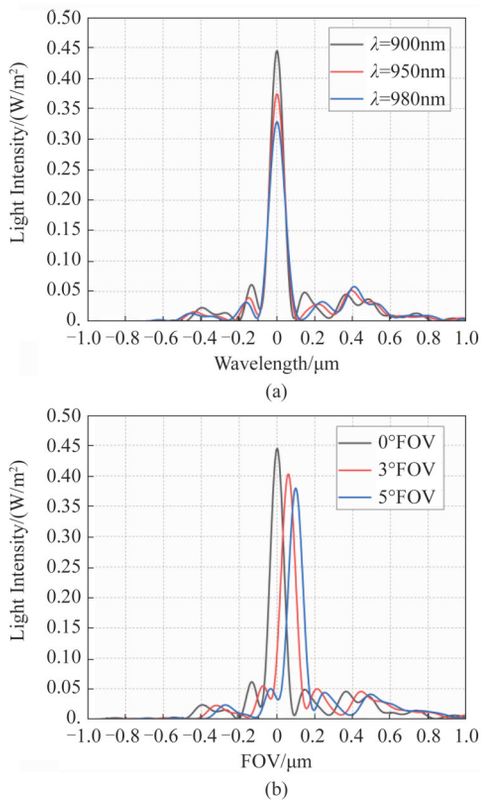

Fig. 8 Focal plane energy distribution, (a) different incident wavelengths, (b) different FOVs
图8 焦平面能量分布, (a)不同入射波长,(b)不同视场

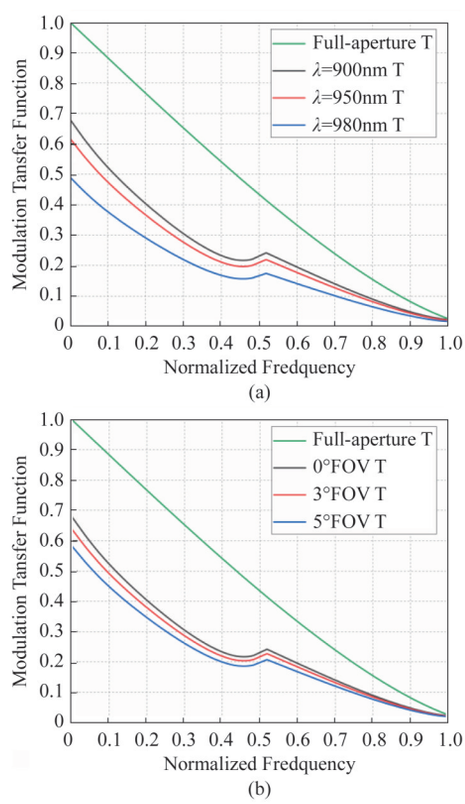

Fig. 9 The degradation of MTF, (a) different incident wavelengths, (b) different Angle of incidence
图9 MTF变化曲线, (a)不同入射波长,(b)不同入射角

Table 2 Simulation parameters of the infrared array-aperture diffraction primary lens
表2 红外合成孔径衍射主镜仿真参数

Wavelength/nm	MTF/(%)	SNR/dB	FOV/(°)	MTF/(%)	SNR/dB
900	45.42	4.92	0	45.42	4.92
950	50.45	6.02	3	48.70	5.14
980	60.64	8.18	5	53.17	5.76

crease gradually, which reflect the spectral and spatial variation characteristics in the image quality degradation. These results are consistent with the theoretical analysis in Section 1, which prove the correctness of the proposed analytical method. In addition, the infrared array-aperture diffractive optical system with the Ring6 and Tri-arm7 structure also have similar imaging characteristics. And the proposed method is applicable to the visible band similarly, while the medium-long wave infrared imaging is not applied to the diffractive imaging system generally for its wide band. Currently, the infrared array-aperture diffractive sensing imaging technology is still in the demonstration stage. The analytical method in this paper can support the optimization design and indicator demonstration of the imaging system, which needs to be further verified in future applications.

3 Conclusions

In this paper, in order to analyze the complex imaging characteristics of the infrared array-aperture diffractive optical system, we establish the MTF and SNR analysis models based on the imaging mechanism of primary lens array-aperture structure and diffraction imaging. Subsequently, considering the primary lens surface microstructure on the subwavelength order, we propose a fast method based on FDTD to solve the diffraction efficiency, and represent the imaging characteristics with the MTF and SNR. The experimental results show that the MTF, the SNR and the diffraction efficiency of the infrared array-aperture diffraction optical system have the characteristics of spectral and spatial variation. When the primary lens filling factor is 0.6, the SNR of the system decreases by 4.92 dB and the MTF area reduces by 45.42%. The correctness and effectiveness of the analytical model are verified by experiments, which can be used as significant references for the application of infrared array-aperture diffractive imaging technology.

References

[1] Zhu L, Wen L, Yang P, *et al*. Aberration correction based on wavefront sensorless adaptive optics in membrane diffractive optical telescope[J]. *Optics Communications*, 2019, **451**:220-225.

[2] Britten J A, Dixit S N, Debruyckere M, *et al*. Large-aperture fast multilevel Fresnel zone lenses in glass and ultrathin polymer films for visible and near-infrared imaging applications[J]. *Applied Optics*, 2014, **53**(11):2312-6.

[3] Kendrick S E, Stahl H P. Large aperture space telescope mirror fabrication trades - art. no. 70102G[J]. *Proceedings of SPIE - The International Society for Optical Engineering*, 2008, DOI: 10.1117/12.788067.

[4] Hyde R A. Eyeglass. 1. Very large aperture diffractive telescopes[J]. *Applied Optics*, 1999, **38**(19):4198-212.

[5] Hyde R A, Dixit S N, Weisberg A H, *et al*. Eyeglass: A very large aperture diffractive space telescope[J]. *Proceedings of SPIE - The International Society for Optical Engineering*, 2002, DOI: 10.1117/12.460420.

[6] Atcheson P D, Stewart C, Domber J, *et al*. MOIRE: initial demonstration of a transmissive diffractive membrane optic for large lightweight optical telescopes[C]. In: Space Telescopes & Instrumentation: Optical, Infrared, & Millimeter Wave. International Society for Optics and Photonics, 2012:21.

[7] Tandy W, Atcheson P, Domber J, *et al*. MOIRE gossamer space telescope - structural challenges and solutions[C] In: 53rd AIAA/ASME/ASCE/AHS/ASC Structures, Structural Dynamics and Materials Conference 20th AIAA/ASME/AHS Adaptive Structures Conference 14th AIAA, 2012.

[8] Tandy W D, Copp T, Campbell L, *et al*. MOIRE gossamer space telescope - Membrane analysis[C]. In: Spacecraft Structures Conference. 2014.

[9] Domber J L, Atcheson P D, Kommers J. MOIRE: Ground Test Bed Results for a Large Membrane Telescope[C]. In: Spacecraft Structures Conference. 2014.

[10] Copp T, Domber J L, Atcheson P D, *et al*. MOIRE: Membrane material property characterizations, testing and lessons learned[C]. In: Spacecraft Structures Conference. 2014.

[11] Atcheson P, Domber J, Whiteaker K, *et al*. MOIRE: ground demonstration of a large aperture diffractive transmissive telescope[C]. In: Space Telescopes and Instrumentation 2014: Optical, Infrared, and Millimeter Wave, 2014, 9143.

[12] Wang D W, Zhi X Y, Zhang W, *et al*. Influence of ambient temperature on the modulation transfer function of an infrared membrane diffraction optical system [J]. *Applied Optics*, 2018, **57** (30): 9096-105.

[13] Jiang S, Zhi X, Dong Y, *et al*. Inversion restoration for space diffractive membrane imaging system[J]. *Optics and Lasers in Engineering*, 2020, 125(Feb.):105863.1-105863.9.

[14] Jiang S, Zhi X, Zhang W D, *et al*. Global Information Transmission Model-Based Multi objective Image Inversion Restoration Method for Space Diffractive Membrane Imaging Systems[J]. *IEEE Transactions on Geoscience and Remote Sensing*, 2021, **60**:1-12.

[15] Zhang S, Wang Y, Zhi X. A novel design of membrane mirror with small deformation and imaging performance analysis in infrared system[J]. *Infrared Physics & Technology*, 2017, **82**:170-177.

[16] Zhang Y, Zheng C, Zhuang Y. Effect of the shadowing in high-numerical-aperture binary phase Fresnel zone plates[J]. *Optics Communications*, 2014, **317**:88-92.

[17] Xu K K. Monolithically integrated Si gate-controlled light-emitting device: Science and properties [J]. *Journal of optics*, 2017, **20**(2):8.

[18] Fiete R D, Tantalo T A, Calus J R, *et al*. Image quality of sparse aperture designs for remote sensing[J]. *Optical Engineering*, 2002, **41**(8):1957-1969.

[19] Buralli D A, Morris G M. Effects of diffraction efficiency on the modulation transfer function of diffractive lenses [J]. *Applied Optics*, 1992, **31**(22):4389-96.

[20] Jiang S, Zhi X, Wei Z, *et al*. Remote sensing image fine-processing method based on the adaptive hyper-Laplacian prior[J]. *Optics and Lasers in Engineering*, 2021, 136(Jan.):106311-6.

[21] Shi S, Prather D W. Vector-based plane-wave spectrum method for the propagation of cylindrical electromagnetic fields[J]. *Optics Letters*, 1999, **24**(21):1445-7.